Biopolymer-based membranes associated with osteogenic growth peptide for guided bone regeneration

Sybele Saska[1,2,5], Suzane C Pigossi[2,3,5], Guilherme J P L Oliveira[2], Lucas N Teixeira[4], Marisa V Capela[1], Andreia Gonçalves[2], Paulo T de Oliveira[4], Younès Messaddeq[1], Sidney J L Ribeiro[1], Ana Maria Minarelli Gaspar[2] and Reinaldo Marchetto[1]

[1] São Paulo State University—UNESP, Institute of Chemistry, Araraquara, SP, Brazil
[2] São Paulo State University—UNESP, School of Dentistry, Araraquara, SP, Brazil
[3] Alfenas Federal University - UNIFAL-MG, School of Dentistry, Alfenas, Minas Gerais, Brazil
[4] Faculty of Dentistry of Ribeirão Preto, University of São Paulo—USP, Ribeirão Preto, SP, Brazil
[5] These authors contributed equally to this paper.

Abstract

Barrier membranes for guided bone regeneration (GBR) mainly promote mechanical maintenance of bone defect space and induce osteopromotion. Additionally, biopolymer-based membranes may provide greater bioactivity and biocompatibility due to their similarity to extracellular matrix (ECM).In this study, biopolymers-based membranes from bacterial cellulose (BC) and collagen (COL) associated with osteogenic growth peptide (OGP(10–14)) were evaluated to determine *in vitro* osteoinductive potential in early osteogenesis; moreover, histological study was performed to evaluate the BC–COL OGP(10–14) membranes on bone healing after GBR in noncritical defects in rat femur. The results showed that the BC–COL and BC–COL OGP(10–14) membranes promoted cell proliferation and alkaline phosphatase activity in osteoblastic cell cultures. However, ECMmineralization was similar between cultures grown on BC OGP(10–14) and BC–COL OGP(10–14) membranes. *In vivo* results showed that all the membranes tested, including the peptide-free BC membrane, promoted better bone regeneration than control group. Furthermore, the BC–COL OGP(10–14) membranes induced higher radiographic density in the repaired bone than the other groups at 1, 4 and 16 weeks. Histomorpho-metric analyses revealed that the BC–COL OGP(10–14) induced higher percentage of bone tissue in the repaired area at 2 and 4 weeks than others membranes. In general, these biopolymer-based membranes might be potential candidates for bone regeneration applications.

1. Introduction

Guided bone regeneration (GBR) is a therapeutical approach in order to promote new bone formation, mainly in periodontal and peri-implant bone defects. GBR is based on biological principle from selective cell exclusion by using an occlusive membrane, which mechanically excludes non-osteogenic cells from the surrounding soft tissues. Hence, the defect space is maintained wherein only bone marrow cells penetrate and promote bone formation [1]. Therefore, this surgical technique induces the osteopromotion inside the osseous wound, i.e., promoting the periodontal tissues regeneration in cases of chronic periodontitis and of peri-implantitis [2]. Actually, the clinical use of membranes has demonstrated predictable clinical results for the treatment of class II molar furcation periodontal lesions [3], for preserving the alveolar ridge architecture following tooth extractions [4] or in association with osseointegrated implants [5].

Among properties required for an ideal GBR barrier membrane include bioactivity, resorption, bio-compatibility and space-maintaining ability during the bone healing process [1]. In this sense, the bacterial cellulose (BC), a natural biopolymer mainly synthesized by *Gluconacetobacter xylinus*, displays special features including a three-dimensional structure consisting of a nanofibers network with higher crystallinity and chemical purity than plant cellulose, in addition to biocompatibility and selective permeability [6]; however its *in vivo* resorption rate is still questionable [7]. Additionally, this nanostructure has a surface morphology close to the extracellular matrix (ECM), which is ideal to favor cell/material interactions. Thereby, BC-based biomaterials have been widely developed to several biomedical applications [8], such as bone [9], cartilage [10] and soft tissues [11]. Furthermore, the BC has also been successful used as a physical-barrier membrane for alveolar bone regeneration in class II furcations in mandibular molars [12, 13] and in association with immediate implants placement [12, 14] or for bone regeneration in critical-size calvarial defects in rats [9, 15].

Considering that collagen (COL) is a major component in ECM, BC–COL composites were synthesized in order to improving biological properties of BC; thereby, affording a bioactivity and a surface morphology closer to ECM to this composite. Indeed, *in vivo* and *in vitro* studies have shown the key role of collagen to different composites [16, 17], whereas collagen plays an important role in cell attachment, mechanical support, and apatite nucleation [18]. Moreover, collagen-based materials have shown proangiogenic qualities and have promoted mesenchymal stem cell osteogenic differentiation as well as alveolar ridge augmentation [19, 20]. Hence, BC–COL composites have been developed as potential candidates for tissue engineering applications [21, 22].

Furthermore, several growth factors regulate the chemotaxis and differentiation of bone-related cells wherein are essential to bone remodeling process [23].Nevertheless, the association of these biomolecules with biomaterials has been proposed to improve osteoconductive and osteoinductive

properties of materials for bone tissue engineering [24, 25]. In this context, osteogenic growth peptide (OGP) and its C-terminal pentapeptide [OGP (10–14)] were chosen as biomolecules for improving osteoconductive and osteoinductive properties of the BC–COL composites. The OGP, an H4 histone-related peptide (H_2N–ALKRQGRTLYGFGG–OH), was isolated from blood during osteogenic remodeling of post ablation marrow regeneration [26]. This peptide is proteolytically cleaved, thus generating the C-terminal penta-peptide (NH_2–YGFGG–OH),named OG(P10–14). Previous studies have established that OGP and OGP (10–14), as a soluble peptide, stimulate the proliferation, differentiation, alkaline phosphatase activity and matrix mineralization in osteoblastic lineage cells [26, 27]. Furthermore, OGP increasing, *in vivo*, bone formation and trabecular bone density [28–30]. OGP-containing bio-materials have exhibited an increase of the osteoblast differentiation/activity as a result a better bioactivity of these biomaterials and a positive effect on bone healing [9, 31].

Hence, the study aimed to evaluate, *in vitro* and *in vivo*, bioactive and osteoinductive properties of the BC–COL composite associated with OGP(10–14) peptide. Considering our previous studies, the BC–COL composite demonstrated higher levels of ALP activity although has shown a delay in the matrix mineralization [21]. In addition, OGP peptides influenced the osteogenic proliferation and favored the mineralization process, conferring an osteoinductive property to the BC membrane [24]. *In vivo* study showed that composites based on BC and hydroxyapatite (HA) associated with OGP peptides are bio-compatible and effective for bone regeneration in critical-size mice calvarial defects [9]. Taken together, OGP(10–14) peptide when associated with the BC–COL composite is expected this material may promote an earlier osteogenic differentiation and an effective bone regeneration. Thus, *in vitro* assays were performed to determine *in vitro* osteoinductive potential in early osteogenesis; moreover, histological study was performed to evaluate the effect of the BC–COL OGP (10–14) membranes on bone healing after GBR in noncritical defects in rat femur.

2. Materials and methods

2.1. BC–COL composites associated with OGP (10–14) peptide

The synthesis of the BC–COL composites was per-formed using carbodiimide-mediated coupling to bind collagen to the glycine-modified BC following the methodology previously proposed by Saska et al [21]. OGP(10–14) peptide was synthesized manually by the solid-phase method and incorporated by adsorption into the never-dried BC–COL composites in accordance with previous methodology described by Saska *et al* [24]. The samples (13 mm in diameter and 5 mm thick) were dried at 37 °C and then sterilized by gamma radiation (20 kGy).

The structural morphology of the BC–COL membranes for GBR was analyzed by scanning electron microscopy (SEM) images with a Philips XL 30 scanning electron microscope. The samples were sputter coated with a 1 nm thick gold layer for 60 s (3 kV and 9.5 mA). The morphology was observed at an accelerating voltage of 10 kV.

2.2. In vitro assays

2.2.1. Cell isolation and primary osteogenic cell cultures

Osteogenic cells were isolated by sequential trypsin/collagenase digestion of calvarial bone from newborn (2–4 days) *Wistar* rats, as previously described [32]. All animal procedures were in accordance with the guidelines of the Animal Research Ethics Committee of the University of São Paulo. Cells were seeded on BC, BC OGP(10–14), BC–COL and BC–COL OGP(10–14) membranes (13 mm in diameter; 20 μm and 70 μmin thick to BC and BC–COL, respectively) at a cell density of 2×10^4 cells/well and cultured for periods up to 21 days using Gibco α-Minimum Essential Medium with L-glutamine (Invitrogen®) supplemented with 10% fetal bovine serum (Invitrogen®), 7 mmol l^{-1} β-glycer-ophosphate (Sigma®), 5 mg ml^{-1} ascorbic acid (Sigma®), and 50 mg ml^{-1} gentamicin (Invitrogen®) at 37 °C in a humidified atmosphere containing 5% CO_2. The culture medium was changed every three days. The progression of cultures was examined by phase contrast microscopy (Axiovert 25, Zeiss, Jena, Germany) of cells grown on polystyrene.

2.2.2. Cell morphology

At days 1, 3, and 7, cell cultures grown on the surfaces of the membranes were fixed for 10 min at room temperature (RT) using 4% paraformaldehyde in 0.1 mol l^{-1} sodium phosphate buffer (PB) pH 7.2. Afterwards, cells were processed for fluorescence labeling for the detection of actin cytoskeleton and cell nuclei. Briefly, they were permeabilized with 0.5% Triton X-100 in PB for 10 min, followed by blocking with 5% skimmed milk in PB for 30 min. Alexa Fluor 488 (green fluorescence)-conjugated phalloidin (1:200, Molecular Probes®) was used to label the actin cytoskeleton. Before microscope observation, the samples were briefly washed with deionized water (dH_2O), and the cell nuclei were stained with 300 nmol l^{-1} 4′6-diamidino-2-phenylindole dihydrochloride, blue fluorescence (DAPI, Molecular Probes, Invitrogen®) for 5 min. Membranes were placed face up on glass slides, covered with 12 mm round glass coverslips (Thermo Fisher Scientific©) and mounted with an antifade kit (Vectashield, Vector Laboratories). The samples were examined by a single examiner blinded under epifluorescence using a Leica DMLB optical microscope (Leica, Germany), with N Plan (×10/12:25, ×20/12:40) and HCX PL Fluotar (×40/0.75, ×100/1.3) objectives, coupled to a Leica DC 300F digital camera. Acquired digital images were processed with Adobe Photoshop software (Adobe Systems).

2.2.3. Cell proliferation and viability

Cell viability/proliferation was evaluated by the [3-(4,5-dimethylthiazol-2-yl)-2,5-diphenyltetrazolium bromide] (MTT, Sigma®).At 10 and 14 days, the culture medium was removed and cells were washed with PBS buffer heated to 37 °C. Then, the cells were incubated in 10% MTT (5 mg ml^{-1}) in 1 ml of culture medium at 37 °C for 4h in a humidified atmosphere containing 5% CO_2. After that,the medium was aspirated and 1 ml of acid isopropanol (0.04 mol l^{-1} HCl in isopropanol) was added to each well. The plates were shaken for 5 min, and 150 μl of this solution was transferred

to 96-well format using opaque-walled transparent-bottomed plates (Thermo Fisher Scientific©). The optical density was read at 570–650 nm on a plate reader (μQuant, Biotek, Winooski, VT), and data were expressed as absorbance.

2.2.4. Evaluation of total protein content, alkaline phosphatase (ALP) activity and mineralized matrix formation

Total protein content of the osteogenic cell cultures was determined at days 14 and 17. The culture medium was aspirated from the wells that were washed three times with PBS at 37 °C. Briefly, the membranes were transferred to a new 24-well culture plates and the wells were filled with 2 ml 0.1% sodium lauryl sulphate (Sigma®). After 30 min, 1 ml of the cell lysate each sample was mixed with 1 ml of Lowry solution (Sigma®) and left for 20 min at RT. Subsequently, 0.5 ml of the phenol reagent of Folin and Ciocalteau (Sigma®) was added and then left for 30 min at RT. Then, the absorbance was measured using a spectrophotometer (CE3021—Cecil, UK) at 680 nm. Total protein content was calculated from a standard curve using bovine serum albumin (Sigma®) giving a range from 25 to 400 μg protein ml^{-1} and the data were expressed as μg proteina ml^{-1}.

ALP activity was assayed in the same lysates used for determining total protein content as the release of thymolphthalein from thymolphthalein monophosphate using a commercial kit (Labtest Diagnostica, Brazil). Briefly, 50 ml of thymolphthalein monophosphate was mixed with 0.5 ml of diethanolamine buffer (0.3 mmol ml^{-1}, pH 10.1) and left for 2 min at 37 °C. The solution was added to 50 ml of the lysates obtained from each well for 10 min at 37 °C. For color development, 2 ml of 0.09 mol l^{-1} Na$_2$CO$_3$ and 0.25 mol l^{-1} NaOH were added. After 30 min, absor-bance was measured at 590 nm, and ALP activity was calculated from a standard curve using thymolphthalein to give a range of 0.012 up to 0.4 μmol thymolphthalein h^{-1} ml^{-1}. Data were expressed as ALP activity normalized against the total protein content.

Mineralized matrix formation was detected at day 21 by Alizarin Red S (Sigma®), which stains areas rich in calcium. Cultures were fixed in 10% formalin for 2 h in RT. After fixation, the samples were dehydrated through a graded series of alcohols (30%, 50%, 70%and 100%) for 1 h in each solution respectively, and the were stained with 2% Alizarin Red S (Sigma®), pH 4.2 for 10 min. Calcium content was evaluated using a colorimetric method [33]. Subsequently, 280 μl of 10% acetic acid was added to each well containing the membranes stained with Alizarin Red S and the plates were incubated at RT for 30 min under shaking. This solution was transferred to a microcentrifuge tube and then vortexing for 1 min. The slurry was overlaid with 100 μl mineral oil (Sigma®), heated at 85 °C for 10 min, and transferred to an ice bath for 5 min. Then, the slurry was centrifuged to 20 000 × g for 15 min and 100 μl of supernatant was transferred to a new microcentrifuge tube. After that, 40 μl of 10% ammonium hydroxide was added to neutralize the acid contained in the solution. This solution containing 140 μl was transferred to 96-well format using opaque-walled transparent bottom plates (Thermo Fisher Scientific©) and then the absorbance was measured on a plate reader (μQuant, Biotek, Winooski, VT) at 405 nm. Data were expressed as absorbance.

2.3. *In vivo* experiments

2.3.1. Surgical protocol

Sixty male adult rats (*Rattus Norvevicus Holtzman*; weigh 200–250 g) were used in this experiment. The animals were randomly divided into three experimental groups with 5 animals each: Group I (GI):BC and BC OGP(10–14), Group II (GII):BC–COL and BC–COL OGP(10–14) and Group III (CG): negative control group (no treatment) for periods at 1, 2, 4 and 16 weeks. All animals were maintained for at least one week prior to surgery in climate controlled rooms at 22 °C, 50% humidity and 12 h light/dark cycles and were fed a standard laboratory diet throughout the study, with ad libitum access to water. All experiments were conducted in accordance with the guidelines established by Brazilian Council of Animal Care (CONCEA) and were approved by Research Ethics Committee of the School of Pharmaceutical Sciences of São Paulo State University-UNESP.

Surgeries were performed using standard aseptic techniques. General anesthesia was induced using intramuscular injections of ketamine hydrochloride (0.1 ml/100 g; Agener União, Brazil) and xylazine hydrochloride (0.01 ml/100 g; Bayer, Brazil). After shaving and preparation of the femoral region, lateral incisions to midline of approximately 10 mm were made on region. After subperiosteal dissection, the femurs were exposed and a noncritical size bone defect (2 mm in diameter) was created in the diaphysis of the each femur. These bone defects were created using first a dental-implant pilot drill and then a dental implant drill (2 mm in diameter; Neodent, Brazil) under constant saline irrigation. The bone defects were created in total thickness of the first cortical until reaching the bone marrow maintaining the integrity of the second cortical bone.

For the Group I, the right femoral defects were recovered by the BC membranes (4mm × 4mm) and the left defects were recovered by the BC OGP(10–14) membranes. In the Group II, the right femoral defects were recovered by the BC–COL membranes and the left defects recovered by the BC–COL OGP(10–14) membranes. For Group III, bone defects were only created in the right femur and these defects were filled with blood clot, no treatment for GBR was performed. The flaps were sutured with 4–0 Vicryl (polygalactin 910 Ethicon, Johnson & Johnson, Brasil) and 4–0 mononylon (Ethicon, Johnson & Johnson, Brazil). In the immediate postoperative period, all animals received an intramuscular administration (single dose) of 0.1 ml kg^{-1} of sodium dipyrone (Ibasa, Brazil). The animals were euthanized at 1, 2, 4, and 16 weeks after surgery by overdose of anesthetics (two to three times the anesthetic dose).

2.3.2. Histological and radiographic analyses

Specimens were harvested, reduced preserving the periosteum and for histological assessment, the defect sites were fixed in 10% formaldehyde solution in PBS for 24 h, the samples were maintained in 70% ethanol. X-ray examination radiographs were taken for all specimens. The analysis aimed to observe the neo-formed bone inside the bone defects. As parameter of analysis, immediate radiographs (IR) were taken before the surgical treatment.

The radiographic examinations were performed by a digital system DenOptix QST (Gendex Dental Systems, Des Plaines, IL) with phosphor plate (31 × 41 mm) and x-ray machine (Gendex 765DC) using 7 mA; 65 kV and 0.04 s. The distance of the locating cylinder to phosphor plate was standardized at 30 cm. Thus, the bone defects were perpendicularly positioned to phosphor plate. The digital x-ray phosphor plates were scanned at

300-pdi resolution using VinxWin Pro software. The radiographs analyses were performed using VinxWin Pro and Adobe Photoshop 7.0 software. The bone density was measured in pixels from the central region of the neoformed bone defects. Data were converted to mmPb. These density values were compared with the density of lead-scale (0.5–3.5 mmPb) radiographed together the specimens.

Subsequently, the specimens were reduced and decalcified with a solution of 50% formic acid (v/v) and 20% sodium citrate (w/v)(1:1; v/v) for a period up to 30 days. Afterward, routine histological processing was performed for inclusion of the specimens in paraffin and for optical microscopy, and then 6 μm semi-serial sections were stained with hematoxylin–eosin. Sections were analyzed under an optical microscope (Jenaval-Zeiss) coupled to a digital camera (Leica DFC425). A researcher (S.S.) blinded to the experimental groups analyzed the following parameters: mineralized bone quality, evidence of fibrotic tissue formation inside the defect site, angiogenesis, inflammatory reaction and membrane degradation.

2.3.3. Histomorphometric analysis

Histomorphometric analysis was performed to measure the following parameters: 1. the defect width in external cortical, 2. the repaired tissue area, and 3. percentage of the newly formed bone. Five blades containing five histological 6 μm thick sections were evaluated for each specimen. Five equally semi-serial sections were evaluated (30 μm distance between the cuts) per animal. The first cut to be evaluated in each specimen was determined by drawing. Then, the digital images (50× magnification) were analyzed by an image analysis software (Image J, Jandel Scientific San Rafael, USA).

2.4. Statistical analysis

The experimental results are expressed as mean and standard deviation (SD). The Kolgomorov–Smirnov test was used to assess the normality of the data and Levene's test for homogeneity. Non-parametric Kruskal–Wallis test followed by Dunn's post hoc test was applied to the data of primary osteogenic cell cultures and for the histometry data. The two-way ANOVA followed by Tukey's test were use to evaluate the radiographic data. The examiner's calibration of the histometric analysis was determined by applying the Spearman correlation test after the re-evaluation of 10% of the samples. These tests showed that the examiner presented r correlation coefficient > 0.91 for all analysis. All statistical analyses were performed using GraphPad Prim 5 (San Diego, CA, USA). Differences were considered statistically significant when $p < 0.05$.

3. Results and discussion

A wide variety of biopolymer-based biomaterials have been proposed for different tissue engineering applications. Among these materials, the collagen-based materials have demonstrated excellent biological properties, such as better tissue-material interactions and cell adhesion, besides working as artificial biomimetic extracellular matrices for GTR [34]. Considering that around 90% of bone matrix protein content is type I collagen, collagen-based materials may provide the innate biological information required for cell adhesion, proliferation and orientation, and promote the chemostatic response [35]. In the last decades, collagen-based biomaterials have been developed for improving mechanical and swelling properties when implanted *in vivo* due to high hydrophilicity of collagen [36]. However, collagen may be easily modified by reaction of its functional groups, introducing cross-links or grafting biological molecules or polymers to create a wide variety of materials with tailored mechanical or biological properties for interest application of the respective biomaterial. Thereby, BC, which has become one of the most attractive biopolymers for tissue engineering [8], was functionalized with collagen via carbodiimide-mediated coupling as an approach for mimicking the ECM environment and for improving biological properties of BC whereas the BC nanofibrillar structure is similar to ECM [21]. Thus, BC–COL nanocomposites were successfully obtained by carbodiimide-mediated coupling and then these composites associated or not with OGP (10–14) peptide were evaluated for bone regeneration, in this study.

Figure 1 shows typical SEM images of dried BC, BC–COL and BC–COL OGP(10–14) membranes. Figure 1(B) shows SEM image of the surface morphology of BC–COL composite wherein collagen filled and homogeneously covered the BC membrane structure (figure 1(A)).BC–COL membrane revealed a compact surface with the filling of surface pores. Indeed, this is an important feature for a barrier membrane for GBR. SEM cross-section images of the BC and BC–COL OGP(10–14) membrane show BC fibers were covered with collagen and oriented in layers (figures 1(E) and (F), respectively). SEM images of the surface morphology of BC–COL OGP(10–14) composite are shown figures 1(C) and (D). These SEM images showed that the peptide incorporation by adsorption, in aqueous solution, slightly changed the surface morphology of this membrane revealing a slightly less occlusive surface, whereas BC fibers more apparent than BC–COL membranes. Therefore, both BC–COL and BC–COL OGP(10–14) membranes might favor the function of cell occlusion excluding the surrounding soft tissues besides protect the blood clot in the bone defect, thereby promoting osteopromotion. Since, the surface morphology of these membranes presented a well-interconnected layer structure and a large surface area necessary for cellular attachment, and vascularization. However, BC–COL composite might potentially stimulate cell growth, and these bar-rier membranes might be material candidate for GBR.

3.1. Cell cultures experiments

3.1.1. Evaluation of cell morphology, cell viability/proliferation, total protein content, ALP activity and mineralized matrix formation

Cell morphology analyzes by means of epifluorescence revealed that cells grown on BC, BC OGP(10–14) and BC–COL were adhered and mostly exhibited a round shape morphology at day 1, while some cells exhibited initial stages of cell spreading (figures 2(A)–(C)). Interestingly, at the same time point, some osteoblastic cells cultured on BC–COL OGP(10–14) showed a fusiform morphology (figure 2(D)). At day 3, a great number of cells was detected on BC–COL and BC–COL OGP(10–14) when compared with the cell population noticed on BC and BC OGP(10–14).

Cells cultured on all membranes exhibited a predominantly stellate/fusiform morphology (figures 2(E)–(H)). At day 7, all membranes showed cell confluence and areas of cell multilayering (figures 2(I)–(L)). The MTT assay indicated no differences among the groups at day 10 ($p = 0.276$). However, osteoblastic cells cultured on both BC–COL membranes exhibited higher cell viability/proliferation compared with BC and BC OGP (10–14) at day 14 ($p = 0.001$)(figure 3(A)).

Total protein content detected in all membranes was similar between 14 and 17 days ($p = 0.418$). However, a greater protein synthesis was observed in BC–COL and BC–COL OGP(10–14) at day 17 ($p = 0.002$)(figure 3(B)). Cells grown on BC–COL and BC–COL OGP(10–14) showed higher ALP activity compared with BC and BC OGP(10–14) at 14 and 17 days ($p = 0.001$)(figure 3(C)). Osteogenic cultures grown on BC membrane showed higher calcium content compared with other membranes ($p = 0.001$) at day 21. BC OGP(10–14) and BC–COL OGP(10–14) exhibited similar levels of calcium content ($p = 0.913$)(figure 3(D)).

In vitro analyzes revealed that all membranes supported cell proliferation and ALP activity. However, osteoblastic cells cultured on BC–COL and BC–COL OGP(10–14) exhibited a high cell proliferation and ALP activity compared with compared with BC membranes associated with or without peptides. These findings could be attributed, at least in part, to collagen and OGP peptide. Indeed, collagen-based scaffolds promote the differentiation of osteoblasts from mesenchymal stem cells (MSCs) and during this process; a high level of osteocalcin and ALP activity has been detected [19]. Concerning OGP(10–14) peptide, some studies have been demonstrated that this molecule is able to increase ALP activity in primary human osteoblast and MSCs cultures [27, 37]. Moreover, OGP(10–14) positively regulates bone formation by stimulating the differentiation of rat MSCs into osteoblasts and concurrently inhibiting adipocyte differ-entiation [27].

ALP is a key enzyme in osteogenesis and exerts an important role in ECM mineralization [38]. In the present study, high levels of ALP activity were observed in cultures grown BC–COL and BC–COL OGP(10–14). Interestingly, this great ALP activity did not reflect in high ECM mineralization. This lack of correlation between ALP activity and mineralization has been described previously [39]. Beck *et al* [39] showed that alkaline phosphatase activity (ALP) is a requirement for mineralization process, however they reveal that mineralization can proceed successfully with a sub-basal level of ALP activity. On the other hand, the failure of mineralization was associated with the repression of osteopontin expression, suggesting an osteopontin requirement for the mineralization process. Additionally, a review literature regarding osteogenic assays using calvarial cells, calvaria-derived cell lines, and bone marrow stromal cells, revealed that in all of these cell types, ALP activity shows similar progression over time using a variety of osteogenic and mineralizing media conditions; however, levels of ALP activity are not proportional to observed mineralization levels [40]. In this way, they suggested that alkaline phosphatase activity might not be the primary screening parameter for selecting a bone-regenerating agent, once the mineralization can occur in the absence of its induction. Despite this apparent unfavorable result in terms of matrix mineralization, the incorporation of collagen and OGP(10–14) into BC membranes may reduce the period of time required to bone regeneration.

3.2. In vivo experiments

The results revealed that all the membranes tested promoted a better bone regeneration compared with the control group (no treatment) and were effective for GBR. Considering that, in general the BC–COL OGP (10–14) membranes were more effective for bone regeneration *in vitro* and *in vivo* in comparison with the others membranes.

3.2.1. Radiographic analysis

At 1 week, the BC–COL OGP(10–14) membranes showed to be more effective for bone healing inasmuch as higher radiographic density values were measured for this treated group compared with other membranes (table 1; figure S1 is available online at stacks.iop.org/BMM/13/035009/mmedia). However, the treated group with BC–COL membrane showed similar radiographic density in relation to the control group (CG) and lower density in comparison with the other experimental groups. After 2 weeks, the BC–COL and BC–COL OGP(10–14) groups showed no difference statistic compared with the CG (table 1). On the other hand, in the GI (BC and BC OGP (10–14)) a lower radiographic density was measured than in the CG and in the GII. The radiographic images showed a cortical bone repaired, wherein observed a well-delimited radiopaque line for bone defects treated with GII membranes, mainly for the BC OGP(10–14) membranes (figure S1). Otherwise, in the CG this well-delimited radiopaque line was only observed at 16 weeks postoperatively.

At 4 weeks, all treated groups showed more radiographic density than the CG; moreover, BC–COL OGP (10–14) membranes induced a higher bone density for newly formed bone in this period compared with other treated groups. At 16 weeks, in all treated groups were measured a higher bone density than the CG. However, OGP(10–14) peptide promoted a better bone density in comparison the peptide-free membranes.

3.2.2. Histological analysis

At 1 week, in the CG was observed the presence of blood clot, fibrous connective tissue and a mild inflammatory reaction inside of the bone defects (figures 4(A) and (B)). Moreover, the beginning of bone healing can be seen on the walls of the bone defects with an osteoid tissue in the mineralization process on the cortical bone. In the medullary cavity, the presence of trabecular bone formation was mainly observed below of the bone defect.

For both experimental groups, GI and GII, presence of trabecular bone formation with active osteoblasts were observed surrounding large medullary spaces filled with mesenchymal tissue inside the bone defects. Furthermore, presence of osteoid was observed adjacent to the membranes and on the wall of the bone defects. Additionally, presence of trabecular bone formation can be seen filling almost all the medullary cavity in the both experimental groups (figures 4(C)–(J)). A mild inflammatory reaction was observed associated with BC and BC OGP(10–14) membranes, and a mild to moderate inflammatory reaction associated with the BC–COL and BC–COL OGP(10–14) membranes at this period.

At 2 weeks, trabecular bone formation in mineralization process (osteoid or immature bone) was observed inside the bone defect (medullary cavity), and adjacent to the periosteum promoting external cortical bone repair, in the CG (figures S2(A) and (B)). Furthermore, no inflammatory reaction was observed in all specimens of the CG. For the experimental groups, GI and GII, an intense bone remodeling was observed close to the newly formed bone inside the bone defect and especially in the medullary cavity for all tested membranes. However, in the GI, this bone remodeling was higher in the bone defects treated with BC membranes in comparison with the BC OGP (10–14) membranes. These findings suggest that the OGP(10–14) peptide promoted a greater stability in bone remodeling process, wherein apparently thicker trabecular bone can be seen for this treated group than for the BC-membrane group (figures S2(C)–(F)). On the other side, the BC–COL and BC–COL OGP (10–14) membranes promoted a better bone healing with a trabecular bone more thick and supposedly more mineralized than in the GI membranes (figures S2(G)–(J)). In addition, GII membranes promoted similar bone repair, corroborating with bone density values. The results suggest that collagen promoted a higher osteoid formation and subsequently mineralization process in comparison with BC; moreover, OGP(10–14) peptide slightly induced a acceleration of bone mineralization and cortical bone formation at this period. A mild inflammatory reaction was observed in all specimens; however, the presence of macrophages was only observed adjacent to BC membrane.

After 4 weeks, in the CG, the bone defects were repaired by a bone in remodeling process compound by a lamellar and woven bone, wherein collagen fibers were in a disorganized way with few concentric lamellae around the Haversian canals and the small medullary spaces enclosed in this tissue; interstitial lamellae were also observed surrounding various blood vessels and osteons (figures 5(A) and (B)). The medullary cavity was repaired with absence of bone trabeculae. However, the new-formed bone was thinner than adjacent bone tissue (figure 5(A)). These findings corroborate with radiographic images wherein showed no well delimited cortical to the bone defects (figure S1). For the experimental groups, the images showed similar histological characteristics to the CG. However the bone repair was in the advanced stages of mineralization, mainly in the OGP(10–14)-containing treated groups, corroborating with radiographic data. Radiographic images revealed cortical bone was fully repaired and well-delimited for OGP(10–14)-containing treated groups (figure S1). Additionally, in the GII, newly formed bone showed collagen fibers were more organized way with concentric lamellae around the osteons and medullary spaces compared with GI (figures 5(C)–(J)). For the BC–COL OGP(10–14) treated group parallel lamellae were observed surrounding external bone cortical, whose histological characteristics refers to lamellar bone (figures 5(I) and (J)). The repaired bones presented similar thickness to the adjacent bone tissue instead of the CG. Furthermore, no inflammatory reaction was observed associated with the membranes. However, some multinucleated cells were observed adjacent to the BC–COL membranes (figures 5(G) and (H)).

At 16 weeks, the bone defects were completely repaired by lamellar bone in all groups, meanwhile only in the CG the repaired bone was less thick in relation to adjacent bone tissue. The membranes were still observed adjacent to the repaired bone tissues, and no difference statistic was observed in relation to reabsorption among periods ($p > 0.05$). Furthermore, no inflammatory infiltrate was observed associated with the membranes; however, few multinucleated cells were observed adjacent to the all membranes (figures S3(C)–(J)).

3.2.3. Histomorphometric analysis

The bone defects were totally closure by woven bone for BC and BC OGP(10–14) groups at postoperative day 7 (figure 6). Moreover, both groups showed statistically superior closure compared with GII and CG ($p = 0.078$). At postoperative day 15, the bone defects were closed with woven bone adjacent to the periosteum (CG) or to the membranes (GI and GII). The CG showed greater defect width followed by the BC–COL and BC–COL OGP(10–14) membranes treated groups, respectively. After 15 days, all the defects presented totally closured.

For total repaired area no difference statistic was measured among the groups for all studied periods, however slight differences can be observed among them (figure 7). At 1 week, the BC OGP(10–14) membrane treated group showed a greater area of tissue repair followed by the BC and BC–COL OGP(10–14) membrane treated groups. The BC–COL treated group and control group showed lower area of repaired tissue at postoperative day 7 (figure 7(A)). At 2 weeks, the BC–COL OGP(10–14) treated group showed a greater area of tissue repair followed by the BC OGP(10–14) and BC membrane treated groups. In addition, the BC–COL treated group and CG showed still lower area of repaired tissue at 15 days, as at post-operative 7 day (figure 7(B)). At 4 weeks, BC OGP (10–14) membrane showed a greater area of tissue repair followed by the BC–COL OGP(10–14) and BC treated groups. In relation to the BC–COL membrane treated group showed a higher area of tissue repair in comparison with CG only after 4 weeks (figure 7(C)). At postoperative day 120, both OGP(10–14)-containing membranes showed a smaller area of repaired tissue similarly to CG. The peptide-free membranes showed a greater area of tissue repair at this period (figure 7(D)). Furthermore, comparing all periods of analysis, the repaired area was gradually reduced for the experimental and control groups, but no statistical differences were observed (figure 7).

Regarding the percentage of bone neoformation in the repaired area, the BC and BC OGP(10–14) treated groups demonstrated a higher percentage of bone tissue in the repaired area than the control group at 1 week ($p = 0.0124$)(figure 8(A)). The membranes with collagen induced a lower percentage of bone neo-formation in the repaired area in comparison with the GI group, however no statistical differences were observed. After 2, 4 and 16 weeks, no statistically significant difference was measured among the groups, although a slight difference can be observed among treatments (figures 8(B)–(D)). After postoperative day 15, the BC membrane treated group showed a lower percentage of bone neoformation in comparison with CG, differently at 1 week. Moreover, the others membranes promoted a greater percentage of bone neo-formation in the repaired area in comparison with CG. The similar results were measured for BC–COL membrane treated group and CG (figure 8(B)). After 16 weeks, all membranes induced a lower percentage of bone tissue in the repaired area in relation to the CG (figure 8(D)). Furthermore, the percentage of bone tissue in the repaired area was gradually increased for all groups during the experiment (figure 8).

In vivo test revealed that all the membranes tested for GBR, including the peptide-free BC membrane, promoted better bone regeneration in comparison with control group in this study. Interestingly, the peptide-free BC membrane promoted the total closure of the bone defects by woven bone at postoperative day 7. This effective result might be associated with the principle of the GBR, meanwhile the BC membrane acts preventing the invasion of fibrous connective inside the bone defect. Therefore, these membranes effectively allowed the maintenance of the bone defect space during the bone healing process. Moreover, BC membranes have demonstrated to be a good potential candidate for bone regeneration. Novaes *et al* evaluated BC membranes for treatment of class II furcation lesions in patients, and reported that BC membrane effectively promoted complete tissue regeneration [41]. Similarly, a clinical study compared the potential of BC and polytetrafluoroethylene membranes for GTR, and this study revealed

that both membranes were effective in treatment for class II furcation lesions in mandibular molars [12]. Moreover, one case report clinically and histologically showed that BC membrane associated with porous hydroxyapatite was effective for the full repair of bone defect associated with a TiAl6V4 implant placed [14].

Additionally, Lee *et al* [15] demonstrated that BC membranes had similar and efficient results regarding new bone formation when compared with collagen membranes on GBR in rat calvarial defects [15]. Similarly, Lee *et al* [42] showed that 0.10 mm BC membrane group demonstrated the greatest permeability, whereas it successfully maintained the defect area without getting reabsorbed until 8 weeks post-operative. In addition, BC membranes ultimately promoted the greatest level of new bone volume (mm3) and new-bone area percentage in comparison with 0.15 mm and 0.20 mm BC membrane groups and the collagen membrane group in rat calvarial defects. In another approach, Lee *et al* [43] evaluated the efficacy of electron beam irradiated BC membranes (EI-BCMs) in comparison with collagen membranes in peri-implant dehiscence defects of beagle dogs. The micro-computed tomography and histometric analyses showed that EI-BCMs were non-significantly different from collagen membranes in terms of new bone area, remaining bone substitute volume and bone-to-implant contact. Overall, these results confirmed the efficacy of BC membrane as a barrier membrane, which secures and maintains space for GBR. Thereby, BC membranes might be used as an alternative biomaterial for bone tissue regeneration.

Comparing the membranes tested in this study, the treated group with the BC–COL OGP(10–14) membranes showed higher radiographic density than the other groups in 1, 4 and 16 weeks. Besides that, for the histomorphometric analyses no difference among the treated groups were measured. However this membrane induced higher percentage of bone tissue in the repaired area in 2 and 4 weeks in comparison to the others membranes. Similarly, the histological analysis showed that the trabeculae bone present in the defect area were more thick and seems more mineralized for BC–COL OGP(10–14) membranes. These findings suggested that this membrane induced the formation of a bone with high quality in the defects area. Furthermore, the OGP(10–14) peptide promoted a bone tissue formation more mineralized at the early periods for both BC and BC–COL membranes, regarding the free-peptide membranes.

The BC membranes associated with OGP(10–14) promoted the total closure of the defects with woven bone after 7 days. On the other hand, the *in vitro* tests showed that this membrane presented an inferior efficacy in comparison to BC–COL OGP(10–14) membrane. These findings suggest that the collagen incorporation to BC associated with the OGP(10–14) peptide promoted a synergic effect on the bone regeneration. Indeed, the OGP(10–14) peptide stimulate the proliferation, differentiation, the alkaline phosphatase activity and matrix associated with OGP(10–14) peptide were previously investigated by Pigossi *et al* [9]. This study showed a upregulation in *Runx2*, *Bglap*, Alpl, *Spp1*, *Tnfrsf11b* bone biomarkers by BC–HA OGP(10–14) membranes, suggesting an acceleration of the osteoblast differentiation/activity with the use of these biomaterials [9].

Taken together, the BC–COL OGP(10–14) composite demonstrated a better efficacy in the bone regeneration of the tibial non-critical-defects considering all methodologies utilized in this study, nevertheless some contradictory results were found. *In vitro* assays, this membrane revealed superior results in comparison to the other membranes, although in the *in vivo* test no major differences were observed among the treated groups. This finding may be associated with a short bioavailability of the peptide in the bone defect microenvironment. Therefore, other methodologies to the peptides incorporation could be performed in future studies to increase the peptide availability in the defect for longer periods. In addition, the BC and BC–COL membranes efficacy should be evaluated in critical defects associated or not with particulate bone filler in future studies to confirm the potential of these membranes to improving the bone regeneration on GBR.

In conclusion, biopolymer-based membranes containing COL and OGP(10–14) peptides promoted in vitro osteoblast proliferation/activity. *In vivo*, these membranes induced a better bone tissue repair mainly in the early periods than control group and BC membranes. Although, BC membranes increased bone regeneration in the non-critical bone defects accelerating the closure of the defect. Thus, the BC–COL OGP (10–14) membranes might a potential candidate as a barrier membrane for GBR.

Acknowledgments

References

[1] Ignatius A A, Ohnmacht M, Claes L E, Kreidler J and Palm F 2001 A composite polymer/tricalcium phosphate membrane for guided bone regeneration in maxillofacial surgery J. Biomed. Mater. Res. 58 564–9

[2] Bottino MC and Thomas V 2015 Membranes for periodontal regeneration-a materials perspective Front. Oral Biol. 17 90–100

[3] Kinaia B M, Steiger J, Neely A L, Shah M and Bhola M 2011 Treatment of class II molar furcation involvement: meta-analyses of reentry results J. Periodontol. 82 413–28

[4] Pang C, Ding Y, Zhou H, Qin R, Hou R, Zhang G and Hu K 2014 Alveolar ridge preservation with deproteinized bovine bone graft and collagen membrane and delayed implants J. Craniofac. Surg. 25 1698–702

[5] Wessing B, Urban I, Montero E, Zechner W, Hof M, Alandez Chamorro J, Alandez Martin N, Polizzi G, Meloni S and Sanz M 2017 A multicenter randomized controlled clinical trial using a new resorbable non-cross-linked collagen membrane for guided bone regeneration at dehisced single implant sites: interim results of a bone augmentation procedure Clin. Oral Implants. Res. 28 218–26

[6] Czaja W K, Young D J, Kawecki M and Brown R M Jr 2007 The future prospects of microbial cellulose in biomedical applications Biomacromolecules 8 E276–88

[7] Yadav V, Sun L, Panilaitis B and Kaplan D L 2015 In vitro chondrogenesis with lysozyme susceptible bacterial cellulose as a scaffold J. Tissue Eng. Regen. Med. 9 276–88

[8] Ullah H, Wahid F, Santos H A and Khan T 2016 Advances in biomedical and pharmaceutical applications of functional bacterial cellulose-based nanocomposites Carbohydr. Polym. 150 330–52

[9] Pigossi S C, de Oliveira G J, Finoti L S, Nepomuceno R, Spolidorio L C, Rossa C Jr, Ribeiro S J, Saska S and Scarel-Caminaga R M 2015 Bacterial cellulose-hydroxyapatite composites with osteogenic growth peptide (OGP) or pentapeptide OGP on bone regeneration in critical-size calvarial defect model J. Biomed. Mater. Res. A 103 3397–406

[10] Svensson A, Nicklasson E, Harrah T, Panilaitis B, Kaplan D L, Brittberg M and Gatenholm P 2005 Bacterial cellulose as a potential scaffold for tissue engineering of cartilage Biomaterials 26 419–31

[11] Sulaeva I, Henniges U, Rosenau T and Potthast A 2015 Bacterial cellulose as a material for wound treatment: properties and modifications, a review Biotechnol. Adv. 33 1547–71

[12] dos Anjos B, Novaes A B Jr, Meffert R and Barboza E P 1998 Clinical comparison of cellulose and expanded polytetrafluoroethylene membranes in the treatment of class II furcations in mandibular molars with 6-month re-entry J. Periodontol. 69 454–9

[13] Simonpietri C J, Novaes A B Jr, Batista E L Jr and Filho E J 2000 Guided tissue regeneration associated with bovine-derived anorganic bone in mandibular class II furcation defects. 6-month results at re-entry J. Periodontol. 71 904–11

[14] Novaes A B Jr and Novaes A B 1993 Bone formation over a TiAl6V4 (IMZ) implant placed into an extraction socket in association with membrane therapy (Gengiflex) Clin. Oral Implants. Res. 4 106–10

[15] Lee S H, Lim Y M, Jeong S I, An S J, Kang S S, Jeong C M and Huh J B 2015 The effect of bacterial cellulose membrane compared with collagen membrane on guided bone regeneration J. Adv. Prosthodont. 7 484–95

[16] Liao S, Wang W, Uo M, Ohkawa S, Akasaka T, Tamura K, Cui F and Watari F 2005 A three-layered nano-carbonated hydroxyapatite/collagen/PLGA composite membrane for guided tissue regeneration Biomaterials 26 7564–71

[17] Teng S H, Lee E J, Wang P, Shin D S and Kim H E 2008 Three-layered membranes of collagen/hydroxyapatite and chitosan for guided bone regeneration J. Biomed. Mater. Res. B 87 132–8

[18] Nudelman F, Pieterse K, George A, Bomans P H, Friedrich H, Brylka L J, Hilbers P A, de With G and Sommerdijk N A 2010 The role of collagen in bone apatite formation in the presence of hydroxyapatite nucleation inhibitors Nat. Mater. 9 1004–9

[19] Donzelli E et al 2007 Mesenchymal stem cells cultured on a collagen scaffold: in vitro osteogenic differentiation Arch. Oral Biol. 52 64–73

[20] R Schneider R K, Puellen A, Kramann R, Raupach K, Bornemann J, Knuechel R, Perez-Bouza A and Neuss S 2010 The osteogenic differentiation of adult bone marrow and perinatal umbilical mesenchymal stem cells and matrix remodelling in three-dimensional collagen scaffolds Biomaterials 31 467–80

[21] Saska S, Teixeira L N, de Oliveira P T, Gaspar A M, Ribeiro S J, Messaddeq Y and Marchetto R 2012 Bacterial cellulose-collagen nanocomposite for bone tissue engineering J. Mater. Chem. 22 22102–12

[22] Wiegand C, Elsner P, Hipler U and Klemm D 2006 Protease and ROS activities influenced by a composite of bacterial celluloseand collagen type I in vitro Cellulose 13 689–96

[23] Gautschi O P, Frey S P and Zellweger R 2007 Bone morphogenetic proteins in clinical applications ANZ J. Surg. 77 626–31

[24] Saska S et al 2012 Characterization and in vitro evaluation of bacterial cellulose membranes functionalized with osteogenic growth peptide for bone tissue engineering J. Mater. Sci. 23 2253–66

[25] Shi Q, Li Y, Sun J, Zhang H, Chen L, Chen B, Yang H and Wang Z 2012 The osteogenesis of bacterial cellulose scaffold loaded with bone morphogenetic protein-2 Biomaterials 33 6644–9

[26] Bab I, Gazit D, Chorev M, Muhlrad A, Shteyer A, Greenberg Z, Namdar M and Kahn A 1992 Histone H4-related osteogenic growth peptide (OGP): a novel circulating stimulator of osteoblastic activity EMBO J. 11 1867–73

[27] Chen Z X, Chang M, Peng Y L, Zhao L, Zhan Y R, Wang L J and Wang R 2007 Osteogenic growth peptide C-terminal pentapeptide [OGP(10–14)] acts on rat bone marrow mesenchymal stem cells to promote differentiation to osteoblasts and to inhibit differentiation to adipocytes Regul. Pept. 142 16–23

[28] Sun Y Q and Ashhurst D E 1998 Osteogenic growth peptide enhances the rate of fracture healing in rabbits Cell. Biol. Int. 22 3313–9

[29] Chen Y C, Bab I, Mansur N, Muhlrad A, Shteyer A, Namdar-Attar M, Gavish H, Vidson M and Chorev M 2000 Structure-bioactivity of C-terminal pentapeptide of osteogenic growth peptide [OGP(10–14)] J. Pept. Res. 147–56

[30] Pigossi S C, Medeiros M C, Saska S, Cirelli J A and Scarel-Caminaga R M 2016 Role of osteogenic growth peptide (OGP) and OGP(10–14) in bone regeneration: a review Int. J. Mol. Sci. 17 E1885

[31] Shuqiang M, Kunzheng W, Xiaoqiang D, Wei W, Mingyu Z and Daocheng W 2008 Osteogenic growth peptide incorporated into PLGA scaffolds accelerates healing of segmental long bone defects in rabbits J. Plast. Reconstr. Aesthet. Surg. 61 1558–60

[32] de Oliveira P T and Nanci A 2004 Nanotexturing of titanium-based surfaces upregulates expression of bone sialoprotein and osteopontin by cultured osteogenic cells Biomaterials 25 403–13

[33] Gregory C A, Gunn W G, Peister A and Prockop D J 2004 An Alizarin red-based assay of mineralization by adherent cells in culture: comparison with cetylpyridinium chloride extraction Anal. Biochem. 329 77–84

[34] Ferreira A M, Gentile P, Chiono V and Ciardelli G 2012 Collagen for bone tissue regeneration Acta Biomater. 8 3191–200

[35] Stevens MM 2008 Biomaterials for bone tissue engineering Mater. Today 11 18–25

[36] Charulatha V and Rajaram A 2003 Influence of different crosslinking treatments on the physical properties of collagen membranes Biomaterials 24 759–67

[37] Spreafico A, Frediani B, Capperucci C, Leonini A, Gambera D, Ferrata P, Rosini S, Di Stefano A, Galeazzi M and Marcolongo R 2006 Osteogenic growth peptide effects on primary human osteoblast cultures: potential relevance for the treatment of glucocorticoid-induced osteoporosis J. Cell. Biochem. 98 1007–20 Biochem. 98 1007–20

[38] Allori A C, Sailon A M and Warren S M 2008 Biological basis of bone formation, remodeling, and repair: II. Extracellular matrix Tissue. Eng. B 14 275–83

[39] Beck G R Jr, Sullivan E C, Moran E and Zerler B 1998 Relationship between alkaline phosphatase levels, osteopontin expression, and mineralization in differentiating MC3T3-E1 osteoblasts J. Cell. Biochem. 68 269–80

[40] Hoemann C D, El-Gabalawy H and McKee M D 2009 In vitro osteogenesis assays: influence of the primary cell source on alkaline phosphatase activity and mineralization Pathol. Biol. 57 318–23

[41] Novaes A B Jr, Moraes N and Novaes A B 1990 Uso do BioFill como membrana biológica no tratamento de lesão de furca com e sem a utilização de hidroxiapatita porosa Rev. Bras. Odontol. 47 29–32

[42] Lee Y J, An S J, Bae E B, Gwon H J, Park J S, Jeong S I, Jeon Y C, Lee S H, Lim Y M and Huh J B 2017 The effect of thickness of resorbable bacterial cellulose membrane on guided bone regeneration Materials 10 E320

[43] Lee S H, An S J, Lim Y M and Huh J B 2017 The efficacy of electron beam irradiated bacterial cellulose membranes as compared with collagen membranes on guided bone regeneration in peri-implant bone defects Materials 10 E1018

Table 1. Bone density measurement via radiographic calibration of the new bone formation from the central region of the defects bone.

	Periods (week)			
Groups	1	2	4	16
Control	0.94 ± 0.11^{Aa}	2.06 ± 0.07^{Bb}	2.08 ± 0.02^{Ab}	2.56 ± 0.13^{Ac}
BC	1.39 ± 0.08^{ABa}	1.70 ± 0.12^{ABab}	2.31 ± 0.02^{ABbc}	2.84 ± 0.32^{ABc}
BC OGP(10–14)	1.21 ± 0.09^{ABa}	1.99 ± 0.12^{ABab}	2.52 ± 0.21^{ABb}	3.37 ± 0.15^{Bc}
BC–COL	0.96 ± 0.06^{Aa}	2.05 ± 0.08^{Bb}	2.58 ± 0.13^{ABbc}	3.09 ± 0.24^{ABc}
BC–COL OGP(10–14)	1.55 ± 0.05^{ABCa}	2.12 ± 0.06^{Bb}	2.76 ± 0.11^{ABCbc}	3.42 ± 0.08^{Bc}

Note. Radiographic density value to IR (0.49 ± 0.03 mmPb). Data are reported as mean $\pm$ SD (mmPb); uppercase letters set indicate statistical difference among the groups at the same period; lowercase letters set indicate statistical difference of the same group in relation to the period; ($p < 0.05$).
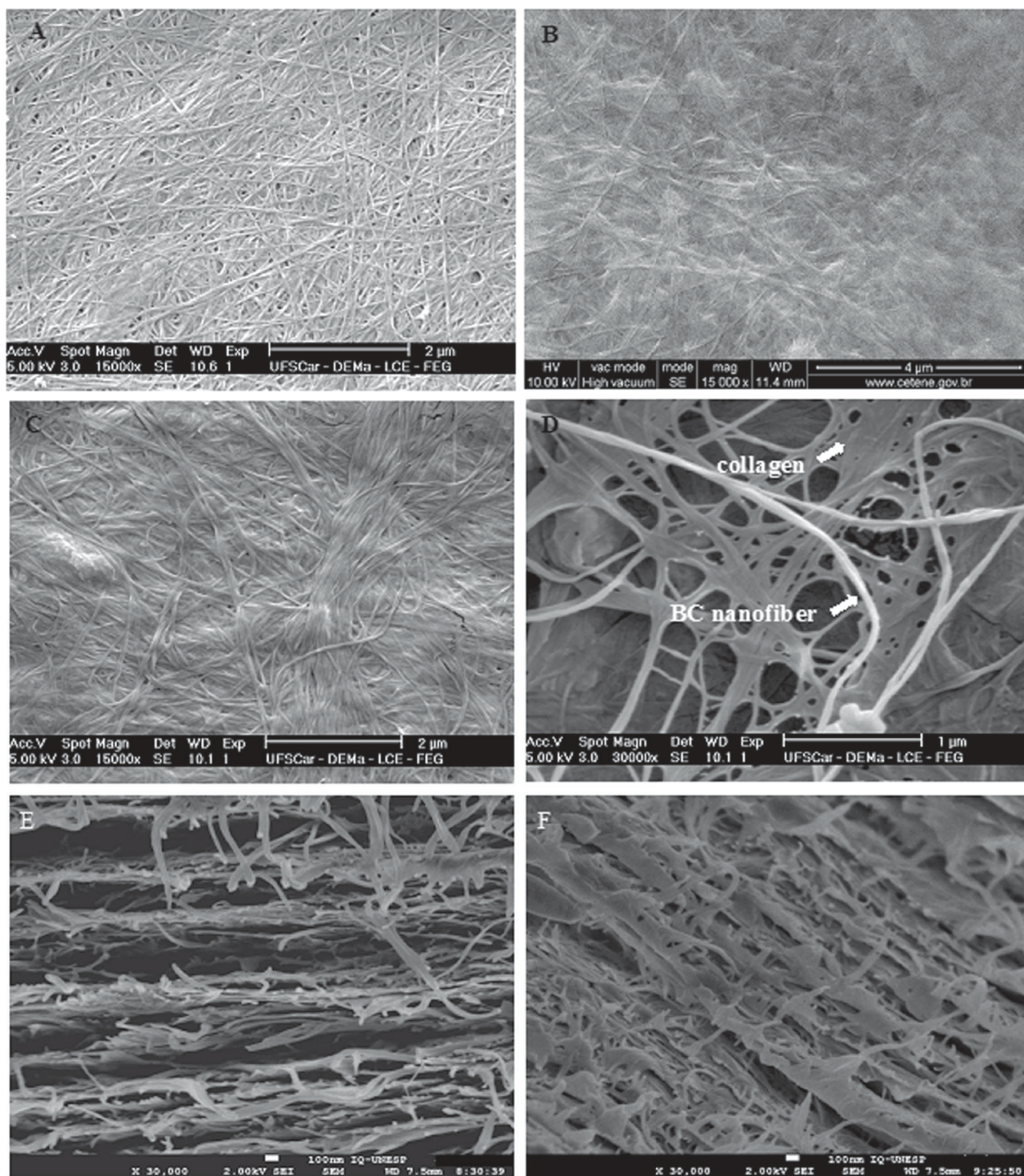
Figure 1. SEM surface images of the BC, BC–COL and BC–COL OGP(10–14) membranes ((A)–(C), respectively; 15 000×); BC–COL OGP(10–14) membrane ((D), 30 000×). SEM cross-section images of the BC and BC–COL OGP(10–14) membranes ((E) and (F), respectively; 30 000×).
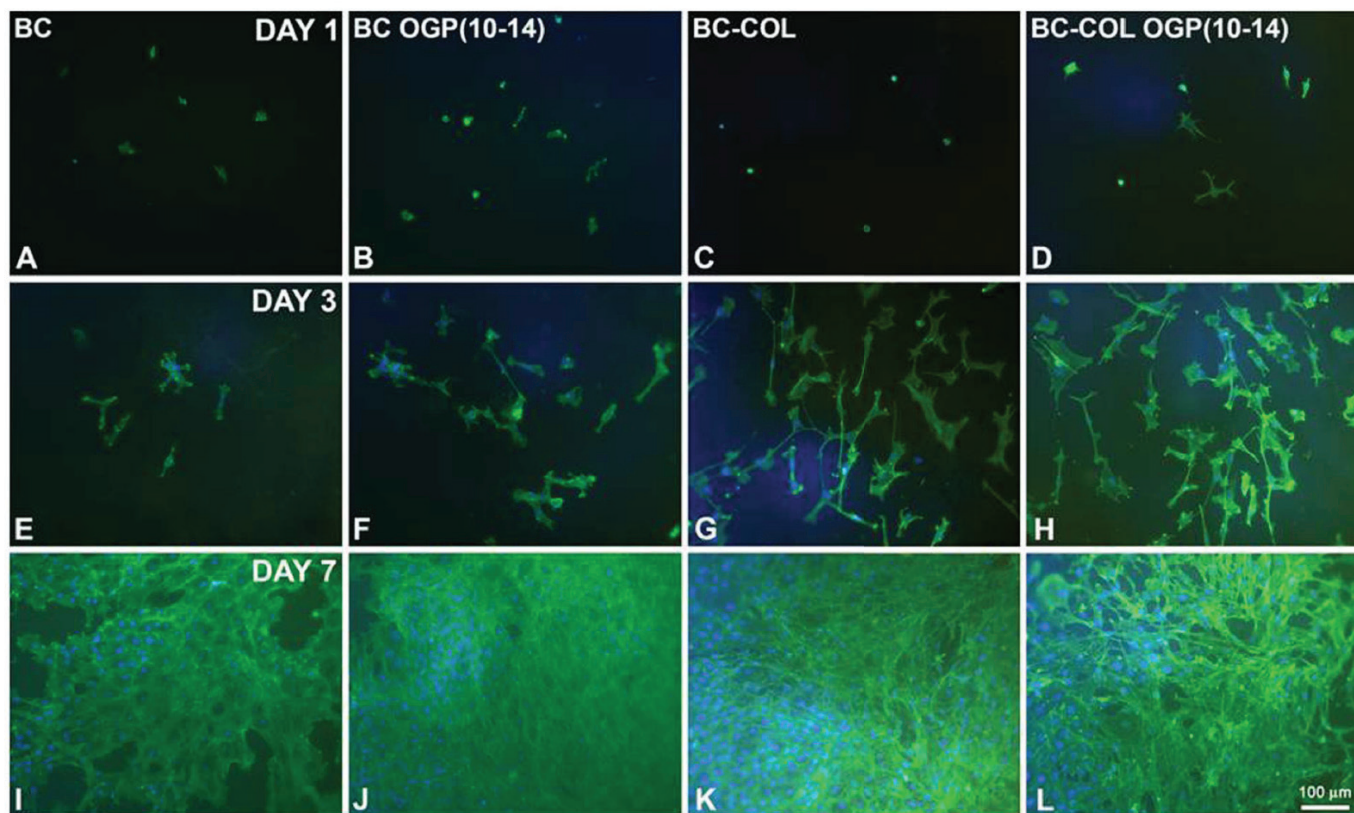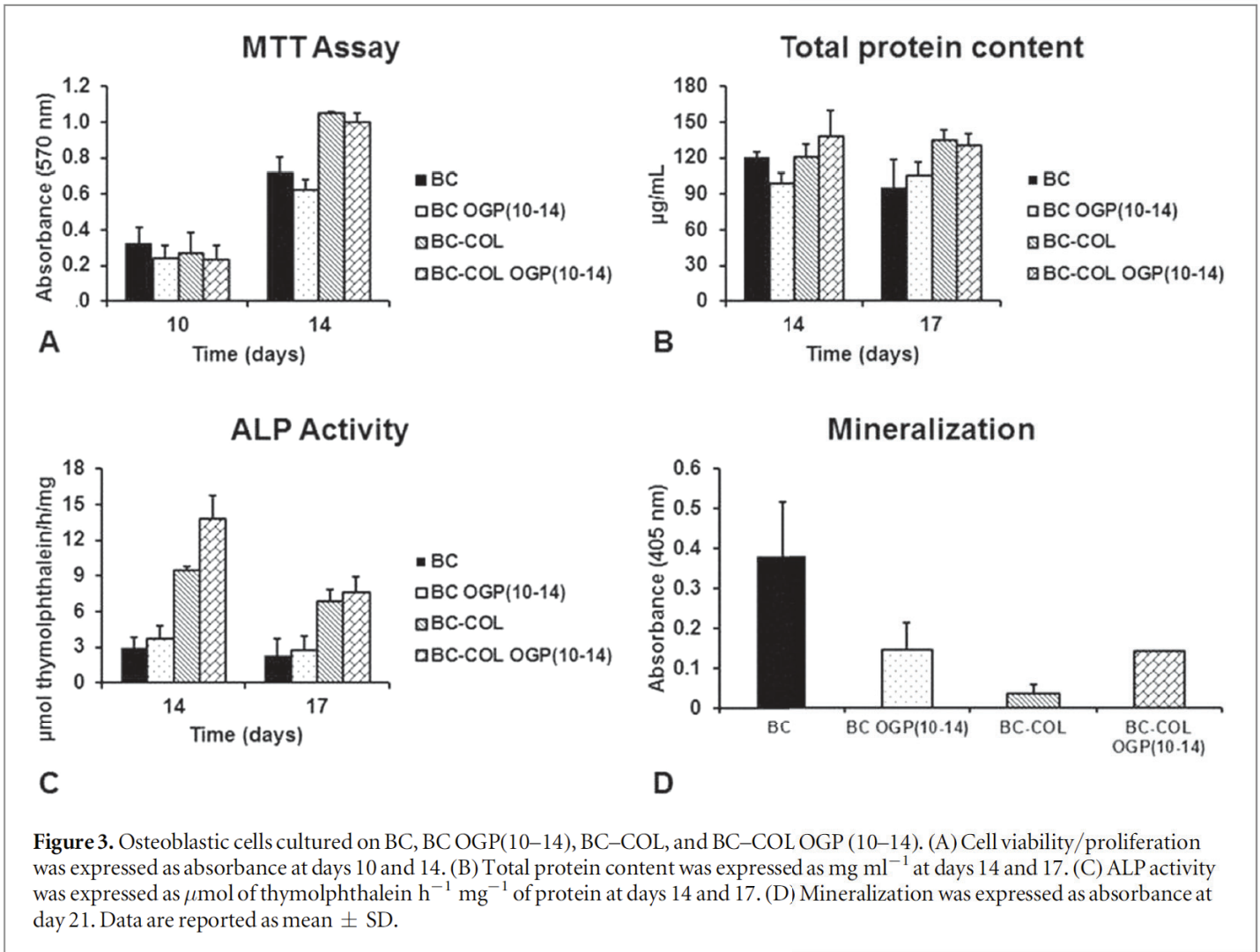
11

Figure 2. Epifluorescence of osteoblastic cells cultured on BC (A), (E) and (I), BC OGP(10–14) (B), (F), and (J), BC–COL (C), (G) and (K), and BC–COL OGP(10–14) (D), (H), and (L) membranes at 1 (A)–(D), 3 (E)–(H), and 7 (I)–(L) days. Green fluorescence (Alexa Fluor 488 conjugated phalloindin) reveals actin cytoskeleton, whereas blue fluorescence (DAPI DNA stain) highlights cell nuclei. Cells cultured on BC, BC OGP (10–14), and BC–COL showed a round shape, while some cells exhibited initial stages of cell spreading at day 1 (A)–(C). In BC–COL OGP(10–14) membranes, at day 1, spreaded cells were promptly observed (D). At day 3, cells grown on all membranes exhibited a predominantly stellate/fusiform morphology (E)–(H). At day 7, all membranes showed cell confluence and areas of cell multilayering (I)–(L). Scale bar = 100 μm.
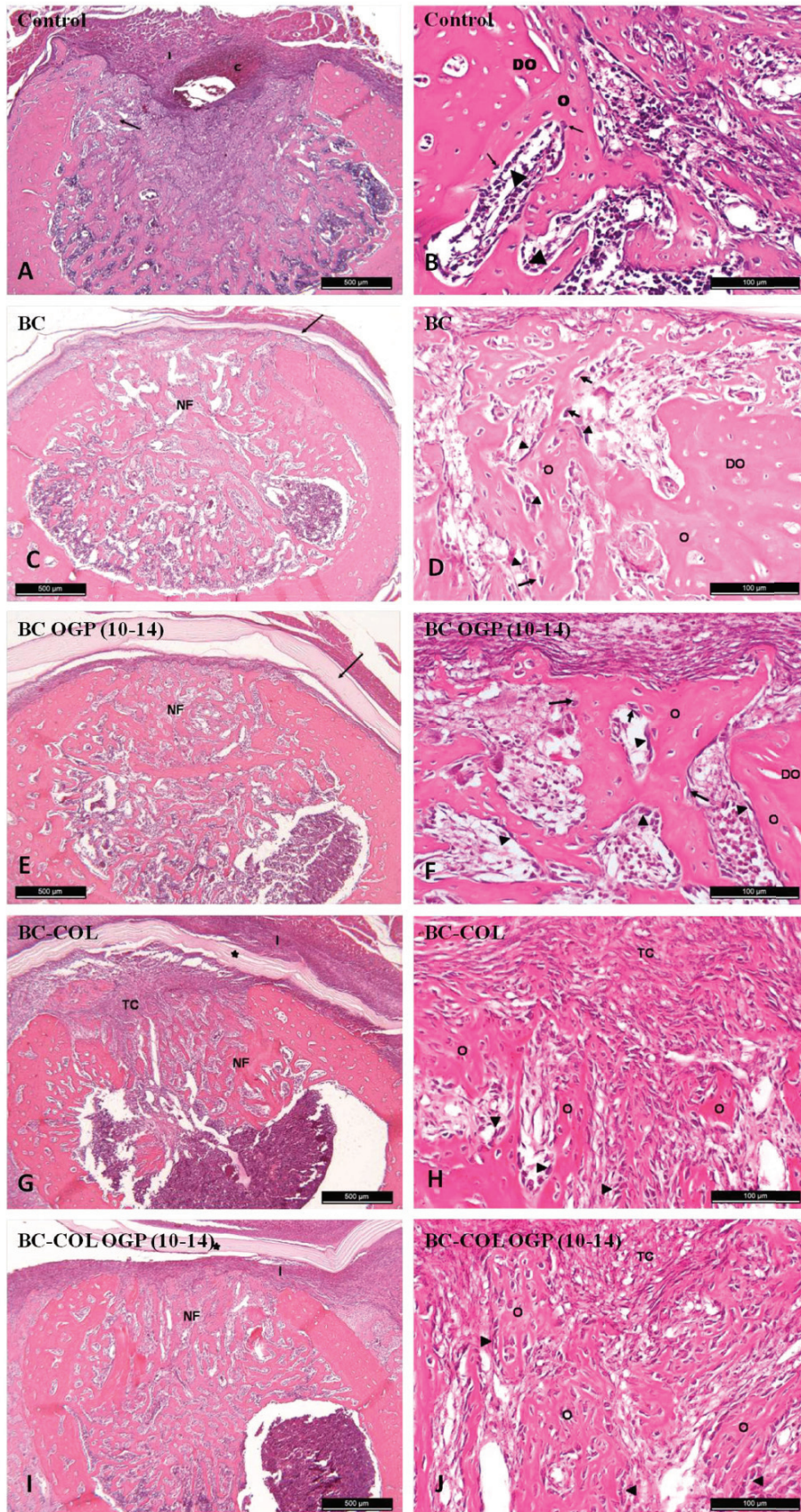
Figure 3. Osteoblastic cells cultured on BC, BC OGP(10–14), BC–COL, and BC–COL OGP (10–14). (A) Cell viability/proliferation was expressed as absorbance at days 10 and 14. (B) Total protein content was expressed as mg ml^{-1} at days 14 and 17. (C) ALP activity was expressed as μmol of thymolphthalein h^{-1} mg^{-1} of protein at days 14 and 17. (D) Mineralization was expressed as absorbance at day 21. Data are reported as mean $\pm$ SD.

Figure 4. Histological photomicrographs of control and membranes groups at 1 week. Inflammatory infiltration (I) and blood clot (C) inside the bone defect; trabecular bone formation (arrow); active osteoblasts (arrowheads); young bone (O) adjacent to the bone defect (DO); osteoid matrix (arrows); immature trabecular bone formation within the defect bone (NF), and also observed the presence of BC membranes (arrows black); hematoxylin–eosin staining (HE), scale bar (100 μm).
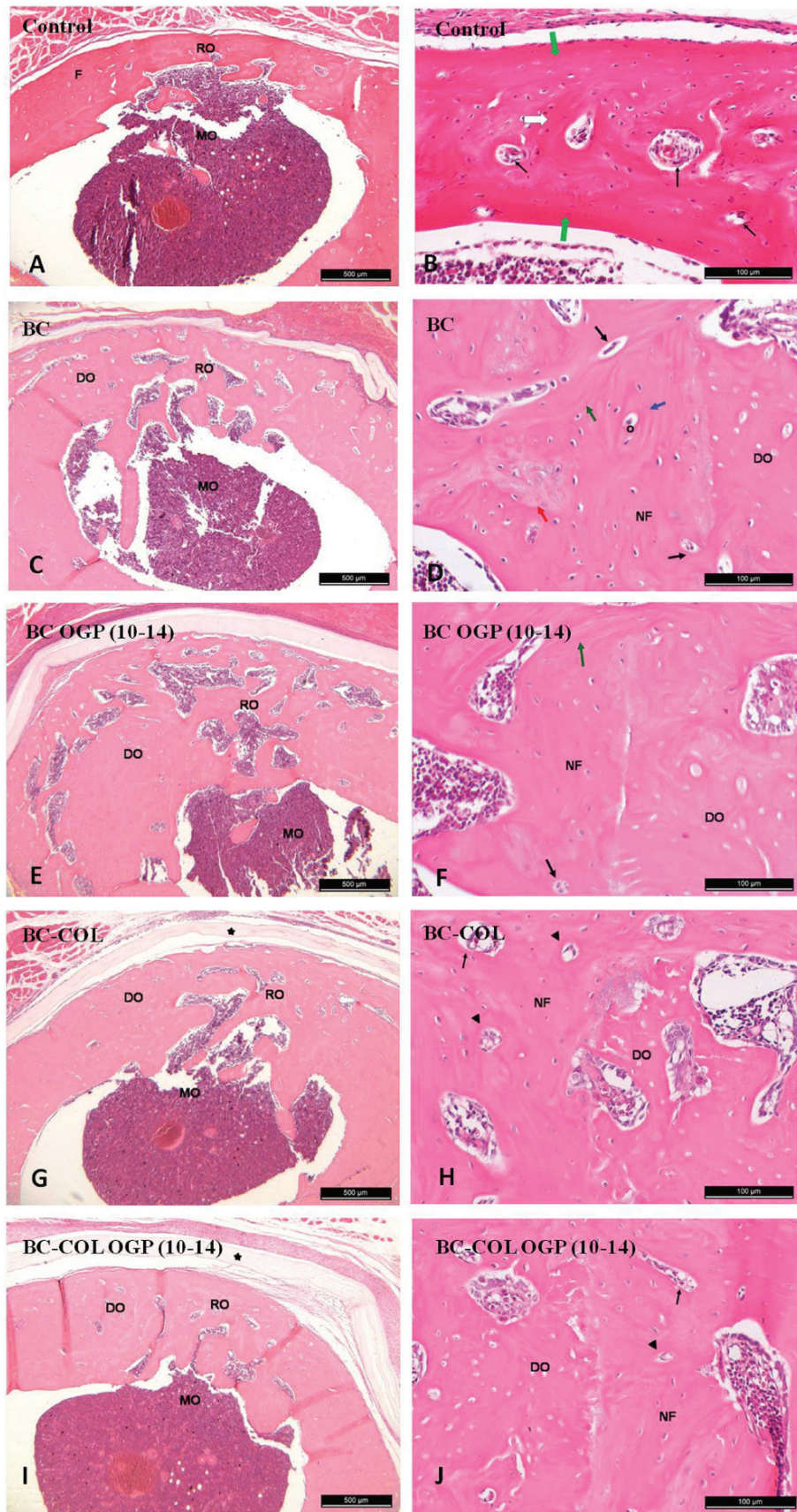
Figure 5. Histological photomicrographs of control and membranes groups at 4 weeks. Bone marrow (MO); femoral bone (F); parallel (green arrow), interstitial (white arrow) and concentric (blue arrow) bone lamellae; repair of bone defect by composite bone (RO); bone defect (DO); blood vessels (black arrows); immature bone trabeculae (T); immature, unorganized collagen fibers inside the bone defect (red arrow); membranes (*); hematoxylin–eosin staining (HE), scale bar (100 μm).
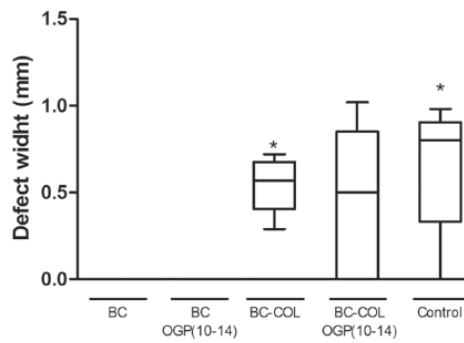
*p<0.05-Higher wide of the defect comparing with the BC and BC OGP(10-14)-Anova c/Tukey

Figure 6. Defect width (mm) data within 1 week in all groups. $^{*}p < 0.05$—groups with opening of the defect greater than the BC and BC OGP(10–14) groups; the ANOVA test followed by Tukey's test. Data are reported as mean $\pm$ SD.
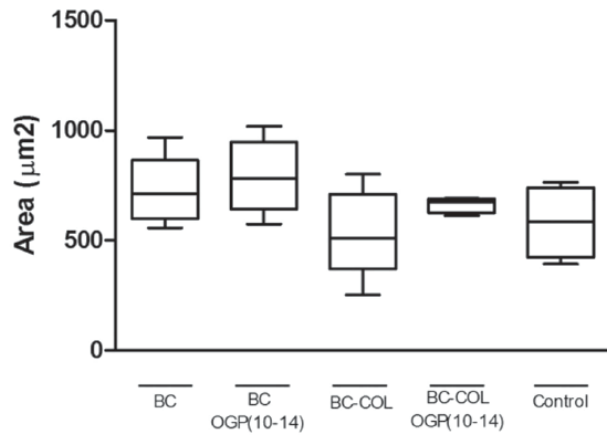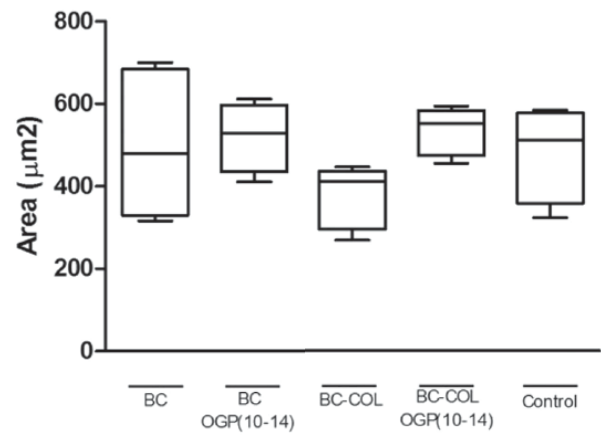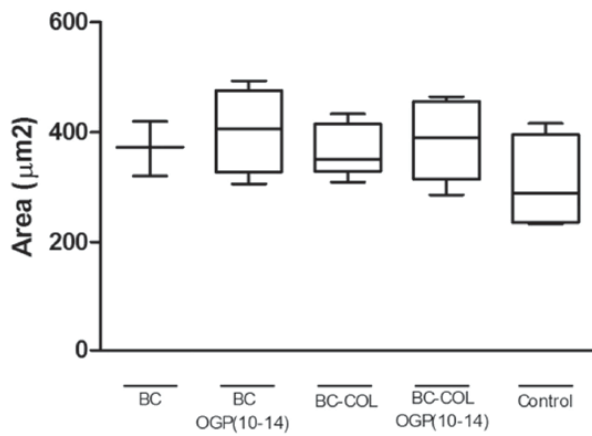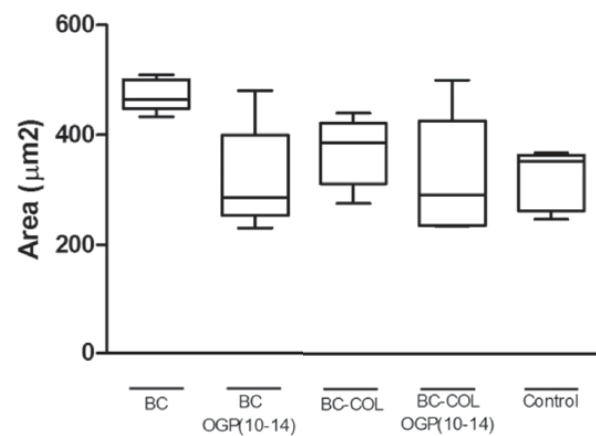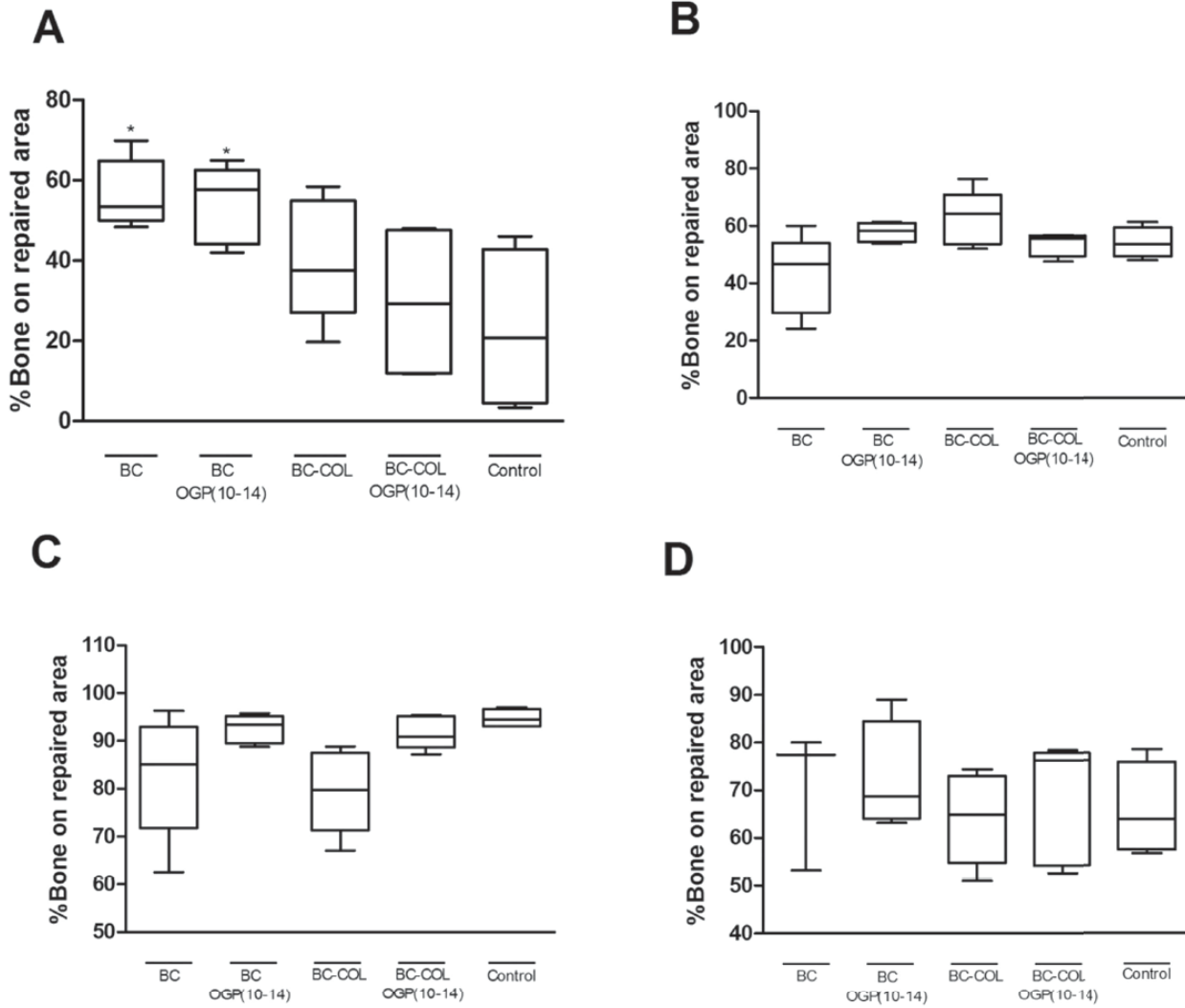
Figure 7. Data area of tissue repaired for all groups. 1 week (A); 2 weeks (B); 4 weeks (C); 16 weeks (D). $^{*}p < 0.05$—groups with a porcentage of bone tissue in the repaired area higher than the control group at 7 days; Kruskal–Wallis's test followed by Dunn's test. Data are reported as mean $\pm$ SD.

* p <0.05- Groups with a porcentage of bone tissue in the repaired area higher than the control-Kruskal-Wallis with Dunn

Figure 8. Percentage of bone tissue data inside the tissue repaired all groups. 1 week (A); 2 weeks (B); 4 weeks (C); 16 weeks (D). $^{*}p < 0.05$—groups with a percentage of bone tissue in the repaired area higher than the control group at 7 days; Kruskal–Wallis's test followed by Dunn's test. Data are reported as mean $\pm$ SD.